

## Supporting information

### Illuminating Solid Gas Storage in Confined Spaces – Methane Hydrate Formation in Porous Model Carbons

Lars Borchardt,<sup>a\*</sup> Winfried Nickel,<sup>a</sup> Mirian Casco,<sup>b</sup> Irena Senkowska,<sup>a</sup> Volodymyr Bon,<sup>a</sup> Dirk Wallacher,<sup>c</sup> Nico Grimm,<sup>c</sup> Simon Krause<sup>a</sup> and Joaquín Silvestre-Albero<sup>b\*</sup>

#### Characterization of model carbon materials

$C_{\text{Micro}}$  is a purely microporous carbon material with slit pores of 0.8 nm (**Fig. 2**). It serves as model for materials that pore sizes are smaller than the elemental cell of the clathrate structure (1.07 nm).  $C_{\text{Micro}}$  is synthesized by the selective etching of Ti atoms out of a TiC powder via hot chlorine gas (carbide-derived carbon approach).  $C_{\text{meso-1}}$  and  $C_{\text{meso-2}}$  are mesoporous carbon materials with spherical pores of 10, and 25 nm, respectively (**Fig. 2**). Their large pores can host several elemental cells of the hydrate crystal structure. The uniform pore size is validated by the type IV isotherm shape with a H1 hysteresis, and also visualized in STEM images (**Fig. 3**). These materials have been synthesized by a hard templating approach starting from monodisperse silica nanoparticles.  $C_{\text{macro}}$  is a macroporous material with cellular pores of approximately 10  $\mu\text{m}$  (**Fig. 3**). These pores can host several thousand of elemental cells of methane hydrate. This material was synthesized via pyrolysis of pine wood.  $C_{\text{micro}}$ ,  $C_{\text{meso-1}}$  and  $C_{\text{meso-2}}$  have comparable particle size of 1-5  $\mu\text{m}$ .  $C_{\text{macro}}$  is a monolithic material of approximately 5 x 5 mm (**Tab.1**) in order to preserve its macropore structure. Specific surface area and pore volume of the materials correlate with their pore sizes, that is the larger the pore volume, the lower the surface area (e.g. 1527  $\text{m}^2\text{g}^{-1}$ , 0.8  $\text{cm}^3\text{g}^{-1}$  for  $C_{\text{micro}}$  and 993  $\text{m}^2\text{g}^{-1}$ , 2.46  $\text{cm}^3\text{g}^{-1}$  for  $C_{\text{meso-2}}$ ) (**Tab.1**). All samples have been loaded with water until saturation. Therefore, the dried samples (degassed at 150 °C in vacuum for 24 h) were placed in a desiccator at 100 % humidity for 3 days. The total water uptake was calculated by mass difference (**Tab.1**). In order to track the water uptake, water vapor adsorption-desorption isotherms were recorded. For  $C_{\text{micro}}$  the water uptake starts rapidly at  $p/p_0=0.5$  and runs into plateau at  $p/p_0 = 0.9$ , indicating full loading under these conditions. The water-accessible pore volume of 0.49  $\text{cm}^3/\text{g}$  is in good agreement with the actual loading of 0.5  $\text{cm}^3/\text{g}$  (**Tab.1**). However, some pores, *i.e.* the smallest and hydrophobic ones are not accessible by water since the pore volume detected by  $\text{N}_2$  is still higher (0.8  $\text{cm}^3/\text{g}$ ). The water adsorption of  $C_{\text{meso-1}}$  and  $C_{\text{meso-2}}$  is shifted to higher  $p/p_0$  due to their larger pore sizes.

Furthermore, no plateau is reached at the highest measureable pressure of  $p/p_0=0.98$ . This reveals the incomplete pore filling up to  $p/p_0=0.98$ . Only 0.3 and 0.25  $\text{cm}^3/\text{g}$  of water is adsorbed at these high pressures, for  $C_{\text{meso-1}}$  and  $C_{\text{meso-2}}$ , respectively. The majority of water first starts adsorbing at higher pressures and reaches values as high as 2.35 and 2.46  $\text{cm}^3/\text{g}$  at 100% humidity, for  $C_{\text{meso-1}}$  and  $C_{\text{meso-2}}$ , respectively. For  $C_{\text{meso-2}}$  this water uptake perfectly matches the accessible pore volume detected by  $\text{N}_2$ -physisorption (**Tab. 1**). The total water uptake of  $C_{\text{meso-1}}$  is higher than the pore volume detected by  $\text{N}_2$ -physisorption, most likely due to interparticular spaces. As expected  $C_{\text{macro}}$  shows the lowest water uptake of 0.29  $\text{cm}^3/\text{g}$ . The pores are too large and too hydrophobic to incorporate water in their entire pore volume. The latter can be estimated to be about 5.5  $\text{cm}^3/\text{g}$  by means of geometrical calculations (**Tab. 1**). Only minor water cluster are adsorbed, preferably at cracks and edges.

#### **About possible subcooling effects during methane adsorption measurements.**

From Figure 6A it is clear that the methane hydrate formation for a given pressure, exhibits a large degree of subcooling with a decrease in the adsorption temperature, preferentially at  $-17^\circ\text{C}$  (calculated subcooling is  $-12^\circ\text{C}$ ). Compared to the other measurements ( $2^\circ\text{C}$ ,  $0^\circ\text{C}$  and  $-9^\circ\text{C}$ ), this is the experiment with the largest difference between the phase equilibrium temperature and the experimental temperature. In the same way, the measurements at  $2^\circ\text{C}$  and  $0^\circ\text{C}$  exhibit lower degree of subcooling (only  $3^\circ\text{C}$ ) in each case. This accounts for the sample  $C_{\text{meso-1}}$ . In the case of the  $C_{\text{micro}}$  sample the subcooling is significant at  $0^\circ\text{C}$  and  $2^\circ\text{C}$  but it is rather zero at lower temperatures ( $-9^\circ\text{C}$  and  $-17^\circ\text{C}$ ). However, a closer look to the adsorption measurements in Figure 4 show that the shift in the threshold pressure to lower values due to the decrease in the adsorption temperature is rather similar in both samples with no clear correlation with previous arguments about subcooling. Even more, the largest different among measurements, in terms of threshold pressure, are at  $0^\circ\text{C}/-2^\circ\text{C}$  range in the  $C_{\text{micro}}$  sample and  $2^\circ\text{C}/-9^\circ\text{C}$  in  $C_{\text{meso-1}}$ , which is more logically associated with the different temperature range to promote the water to ice formation depending in the pore size, and indirectly associated with the different activation energy when dealing with water and ice. Indeed, subcooling cannot fully be excluded, but most probably these effects are related to the impact of the activation energy at lower temperatures.

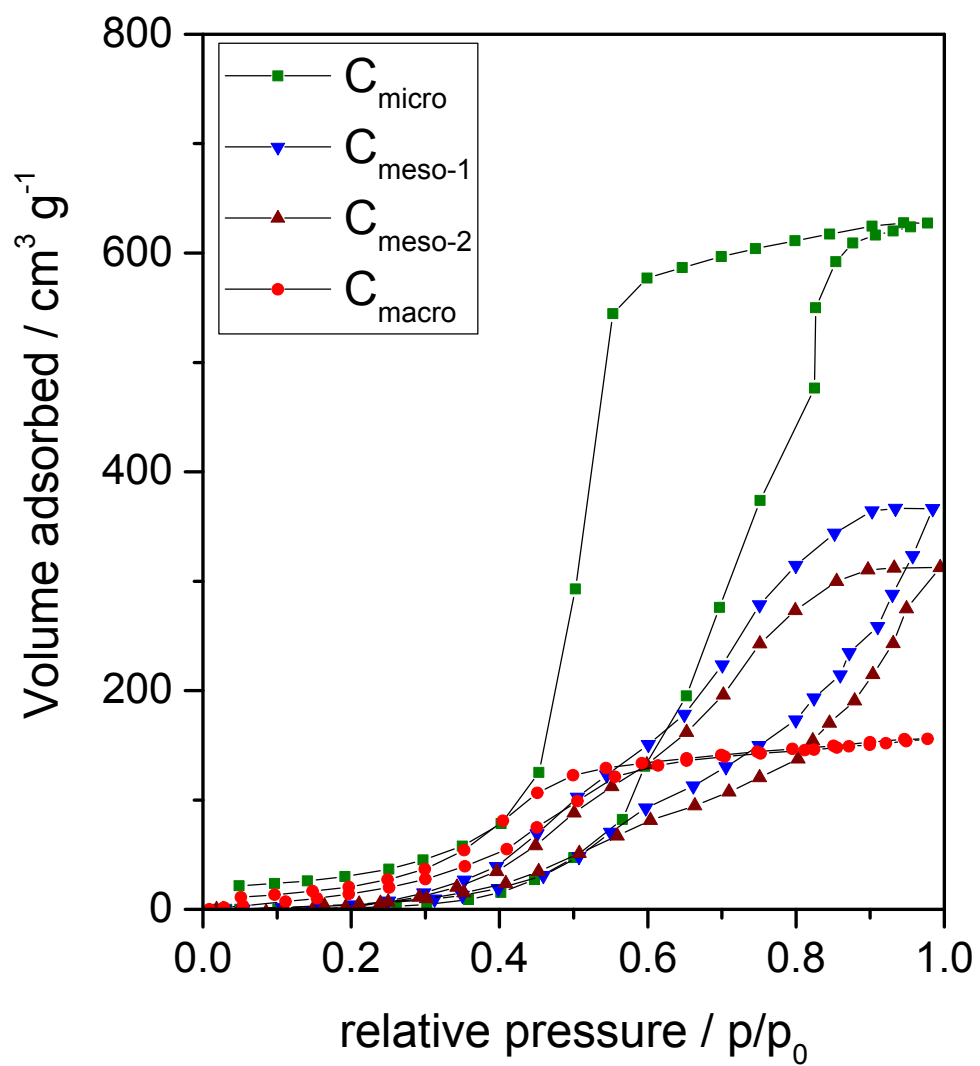
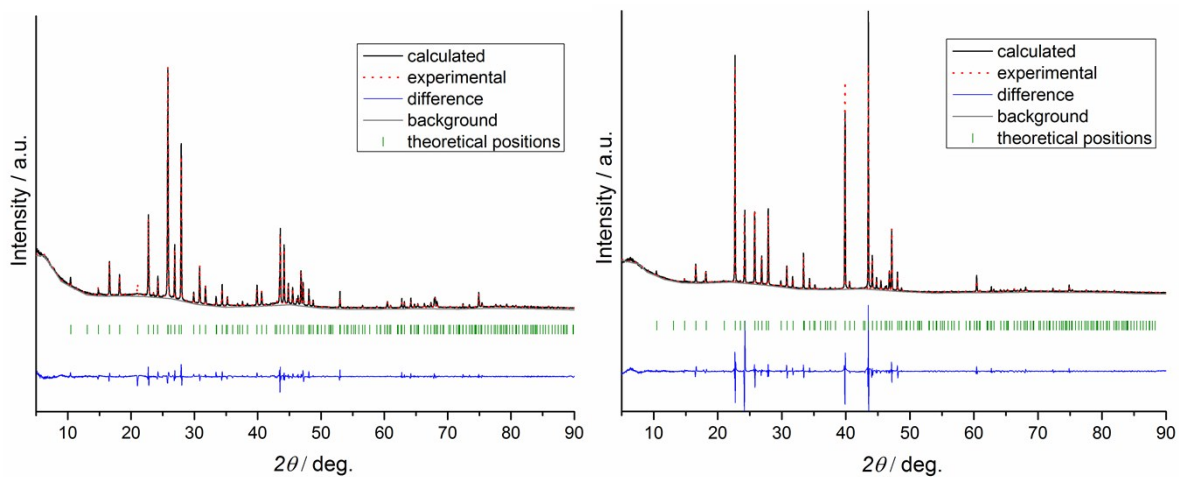
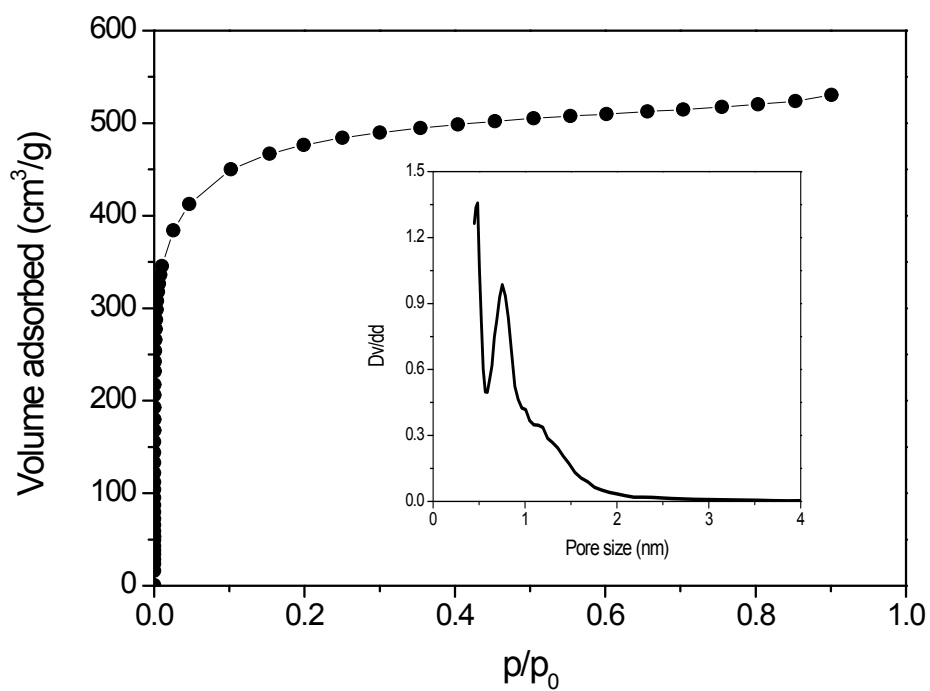


Figure S1. Water adsorption isotherms at 25°C for the different model carbons evaluated.



**Figure S2.** Le Bail fit for Cmico (1 nm) (left) and Cmeso1 (10 nm) (right) samples, loaded with methane at 60 bar at  $-9^{\circ}\text{C}$ . Beside the methane hydrate these results also show the presence of the hexagonal. The origin of the ice crystallite is explained by both freezing of the water in the pores of the investigated material as well as ice crystallites, formed by the freezing of the atmospheric water on the external capillary walls. The last could be confirmed by the presence of Bragg reflections on the 2D detector, originating from the large ice crystallites.



**Figure S3.** Ar adsorption isotherms at -186°C for the C<sub>micro</sub> model material. Pore size distribution (PSD) obtained after application of the QSDFT method (slit pores, equilibrium-model) is included as inset.

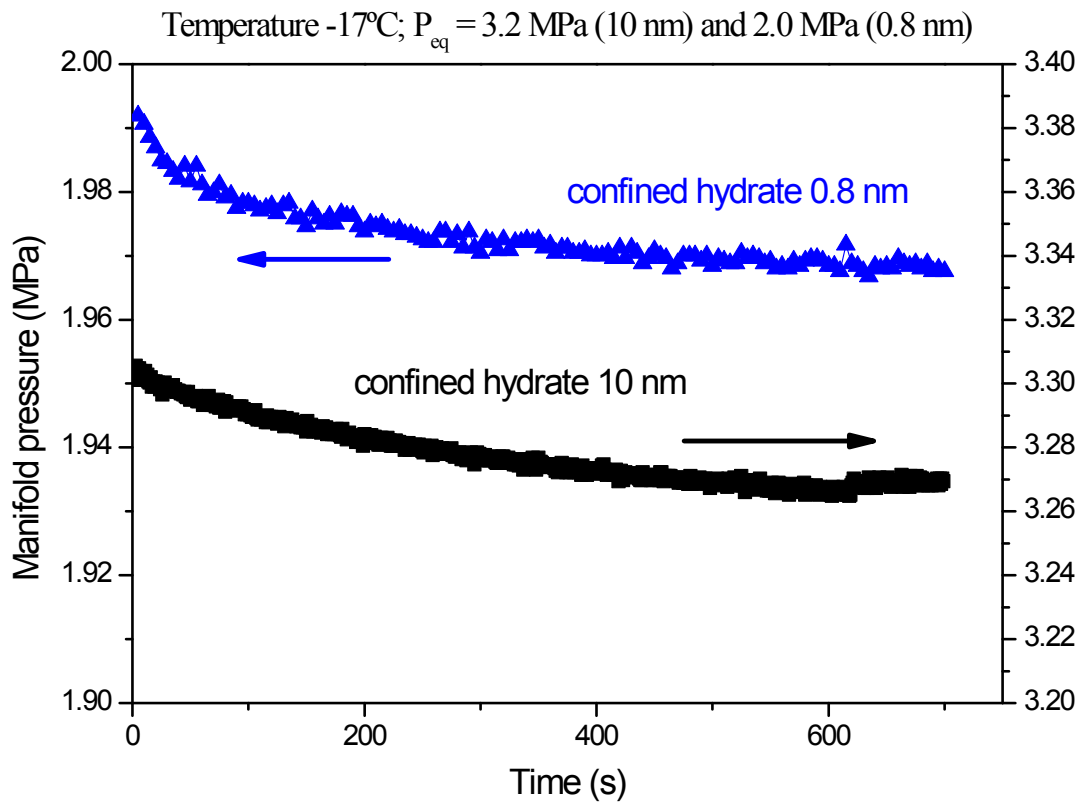


**Figure S4.** Pressure change in the manifold at a specific point of the methane adsorption isotherms (at the methane hydrate nucleation range) at (A) 2°C and (B) -17°C, for samples  $C_{micro}$  and  $C_{meso-1}$ .

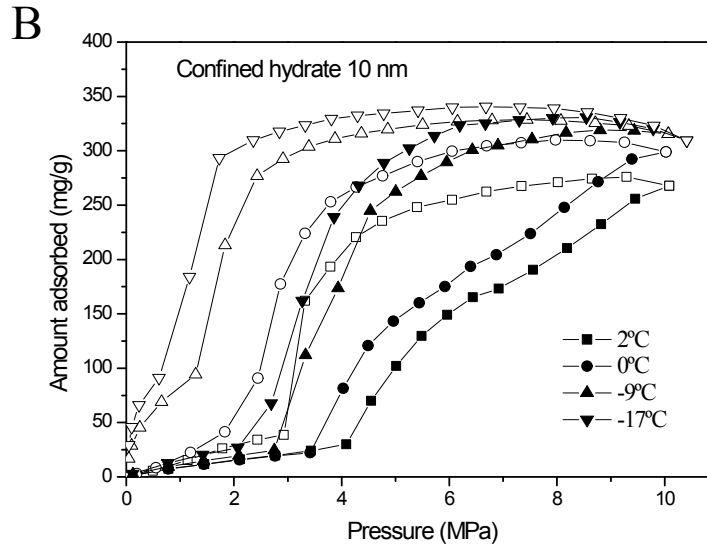
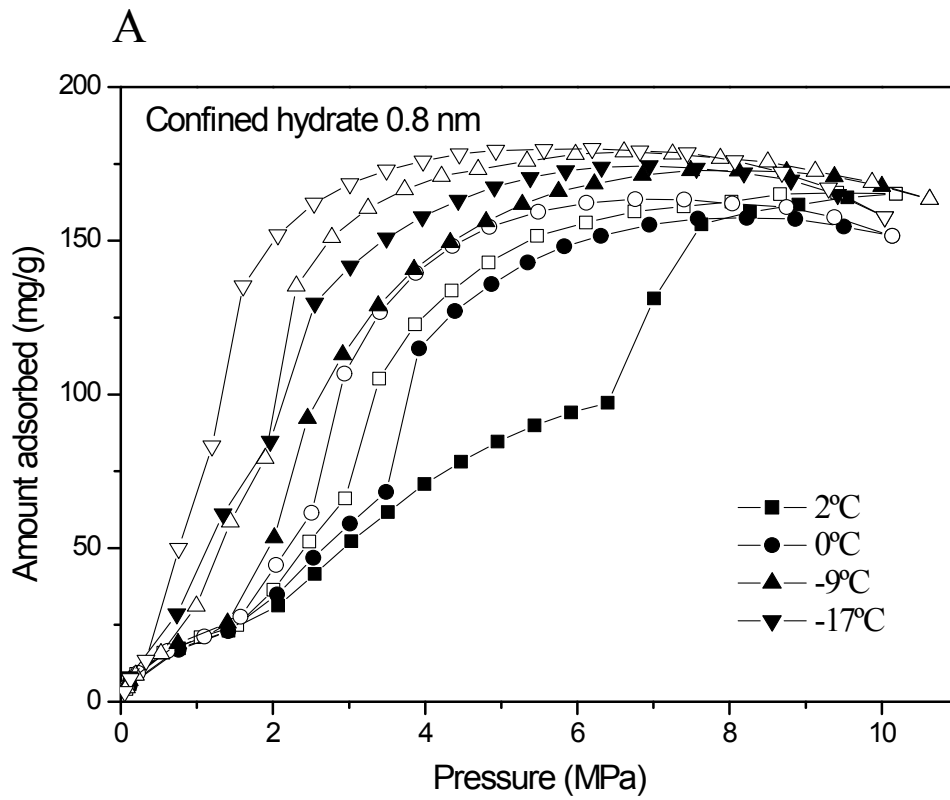


**Figure S5.** Methane adsorption/desorption isotherms of water-loaded (A)  $C_{\text{micro}}$  (mean pore size 0.8 nm) and (B)  $C_{\text{meso-1}}$  (mean pore size 10 nm) samples (saturated) at different adsorption temperatures and up to 10 MPa.

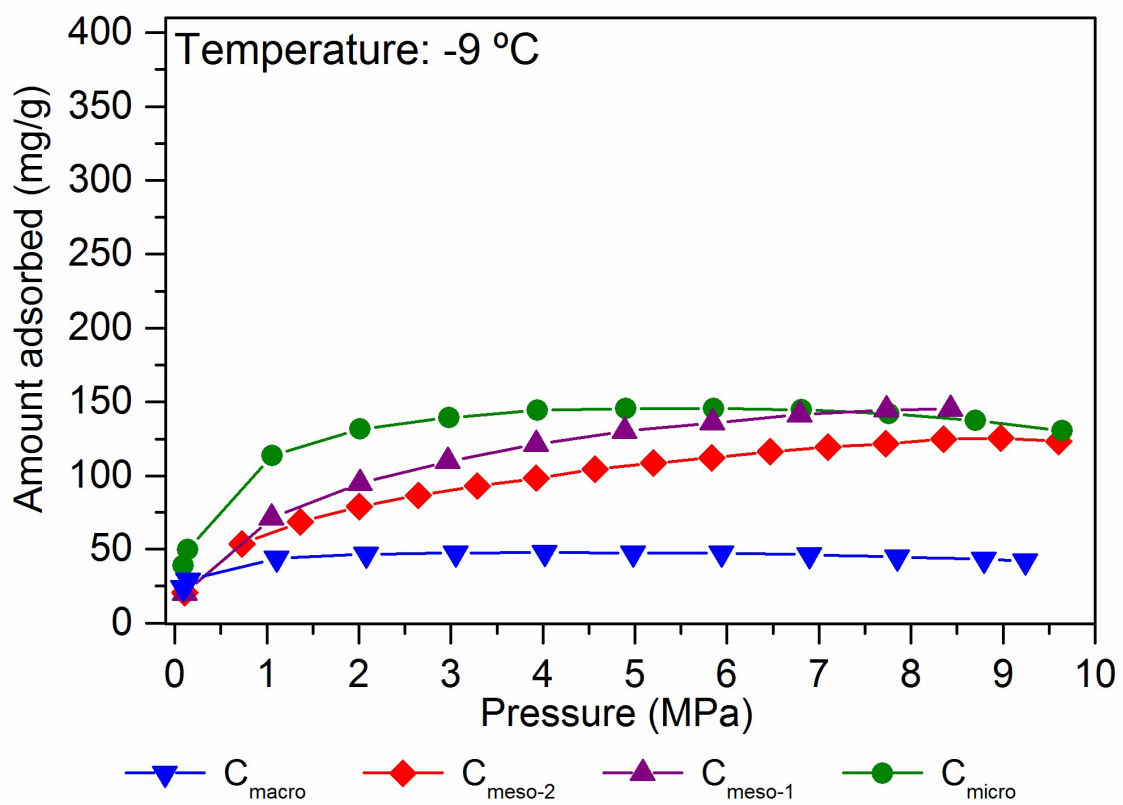


Figure S6. Methane adsorption isotherms of the dry carbon materials at -9 °C and up to 10 MPa.

**Table S1.** Experimental data for profile decomposition for  $C_{\text{micro}}$  and  $C_{\text{meso-1}}$ .

	$C_{\text{micro}}$ (1 nm)		$C_{\text{meso-1}}$ (10 nm)	
	Methane hydrate	Ice	Methane hydrate	Ice
Symmetry, space group	cubic, $Pm\bar{3}n$	hexagonal, $P6_3cm$	cubic, $Pm\bar{3}n$	hexagonal, $P6_3cm$
Unit cell parameter, Å	$a =$ 11.9543(6)	$a = 7.8301(10)$ $c = 7.3574(10)$	$a =$ 11.9604(4)	$a = 7.8292(7)$ $c = 7.3592(6)$
Wave length (Å)	1.5406 (synchrotron)			
$2\theta$ range (°)	5 - 90			
Instrument geometry	Debye-Scherrer			
Zero point line shift (°)	0.02659			
Profile function	Pseudo Voigt			
$U$	0.1312(1)	-0.0243(1)	0.0934(2)	0.1984(1)
$V$	-0.0921(1)	0.0236(1)	-0.0663(2)	-0.1385(2)
$W$	0.0293(1)	0.0115(1)	0.0359(1)	0.0364(1)
Asymmetry correction	Berar-Baldinozzi			
$P1$	0.0924(1)	-0.0240(1)	0.2675(1)	0.3105(1)
$P2$	-0.0221(1)	0.0378(1)	-0.0085(1)	0.0275(1)
$P3$	-0.0057(1)	-0.0291(1)	0.000	-0.0273(1)
$P4$	0.0334(1)	-0.0314(1)	0.0185(1)	-0.0116(1)
Bragg $R$	0.0153	0.0122	0.0186	0.00870
Final $R_{wp}$	0.0532		0.1100	
Final $R_p$	0.0343		0.0582	
$\chi^2$	0.057		4.78	